RSC Advances

PAPER

View Article Online
View Journal | View Issue

Cite this: *RSC Adv.*, 2020, **10**, 42584

Enhancing thermal conductivity of polyimide composite film by electrostatic self-assembly and two-step synergism of Al_2O_3 microspheres and BN nanosheets

Dongxu Liu,[a] Chuanguo Ma,[abc]* Hongtao Chi,[a] Shihui Li,[a] Ping Zhang[c] and Peibang Dai[abc]

To improve the perfection of a three-dimensional thermally conductive network in polyimide (PI) composite film and with respect to the economy and simplicity of processing, a strategy of the two-step synergism of Al_2O_3 microspheres and hexagonal boron nitride (BN) nanosheets was proposed. First, BN nanosheet-coated Al_2O_3 microspheres (Al_2O_3@BN) were prepared by electrostatic self-assembly method for the first step of the synergism. Then, the Al_2O_3@BN&BN/PI composite film containing Al_2O_3@BN and BN was fabricated by a two-step method for the second step of the synergism, and was systematically characterized. With an optimized mass ratio of 2 : 1 of Al_2O_3@BN to BN, the thermal conductivity of the 35 wt% Al_2O_3@BN&BN/PI composite film reached 3.35 W m^{-1} K^{-1}, and was increased by 1664% compared to that of pure PI. The synergism of the Al_2O_3 and BN was the most significant in the Al_2O_3@BN&BN/PI composite film with the thermal conductivity, which was 36.6%, 23% and 22% higher than that of the Al_2O_3/PI, BN/PI and Al_2O_3@BN/PI composite films, respectively. The enhancement mechanism of heat conduction was clearly demonstrated. The BN coated on the surface of Al_2O_3 mainly played a bridging role between the Al_2O_3 and the BN network, which improved the perfection of the thermally conductive network. The Al_2O_3@BN segregated the PI matrix to construct the BN network with the typical segregated structure in the composite film, resulting in an efficient thermally conductive network. This work provided a novel strategy for the preparation of conductive polymer composites.

Received 21st September 2020
Accepted 8th November 2020

DOI: 10.1039/d0ra08048a

rsc.li/rsc-advances

1. Introduction

With the development of lightweight, miniaturized and ultra-thin electronic devices, high-performance thermal management materials and thermal interface materials (TIM) have become one kind of the key materials to meet the heat dissipation requirements of electronic devices.[1–3] Filled thermally conductive polymer composites are an important kind of material due to their simple preparation technology, and their remarkable enhancement effect of the thermal conductivity. Common thermally conductive fillers include carbon black,[4] alumina (Al_2O_3),[5] boron nitride (BN),[6] graphene oxide (GO),[7,8] zinc oxide[9] and silicon carbide.[10] It is difficult to achieve high thermal conductivity at a low filler content with the traditional blending process, while the mechanical property, aging property and thermal property of the corresponding composite will be deteriorated at a high filler content.[11,12] In recent years, in order to solve this contradiction, researchers have proposed four novel strategies. The first is to design new thermally conductive fillers, such as flawless graphene,[13] exfoliated BN nanosheet (BNNS)[14] and BN nanotubes.[15] The second is to construct a three-dimensional thermally conductive network by a novel method, such as electrostatic spinning,[16] chemical vapor deposition (CVD),[17] template method,[18–20] freeze-drying method,[21] and segregated structure method.[22] The third is to decrease the thermal resistance at the heat conduction interface, mainly by increasing the compatibility of the interface[23] and reducing the interface scattering of phonons.[24] The fourth is to make thermally conductive fillers to be oriented by using an electric or magnetic field,[25] directional freezing[26] and shear induction.[27] The resulting composites show anisotropy, and the thermal conductivity in a certain direction can be significantly enhanced.

As an important electronic packaging material, polyimide (PI) has a low inherent thermal conductivity of about 0.2 W m^{-1} K^{-1}. It is usually necessary to prepare the PI composite with high thermal conductivity in practical application, which is a hot topic in current research.[6,7,28] In recent years, the research

[a]*School of Material Science and Engineering, Guilin University of Electronic Technology, Guilin 541004, China. E-mail: machuanguo@guet.edu.cn*
[b]*Guangxi Key Laboratory of Information Materials, Guilin 541004, China*
[c]*Engineering Research Center of the Ministry of Education for Electronic Information Materials and Devices, Guilin 541004, China*

on the preparation of thermally conductive PI composites is mainly focused on the surface modification of the filler,[29] construction of the 3D network based on the template,[30] electrostatic spinning processing[5] and synergism of different fillers. Zhou *et al.*[29] used BN to modify the surfaces of the copper nanoparticles and nanowires to enhance the thermal conductivity and dielectric properties of the PI composite film. Gong *et al.*[30] prepared graphene woven fabrics (GWFs) on a nickel mesh using CVD method, and then built a 3D thermally conductive network using the GWFs as a template, which significantly improved the thermal conductivity of the PI composite films. Xia *et al.*[5] successfully prepared Al_2O_3 nanoparticle-coated polyamide acid (PAA) fiber for the first time with a core–shell structure using coaxial electrospinning technology. The as-prepared Al_2O_3@PI thin film was obtained with an effective thermally conductive network, and also has good thermal and mechanical properties. Song *et al.*[31] found that anisotropic BN and spherical Al_2O_3 or aluminum nitride (AlN) formed a synergistic thermally conductive network structure, thus improving the thermal conductivity of the composite film. Due to its good insulation performance and high thermal conductivity of up to 600 W m^{-1} K^{-1}, BN has been well known as a relatively ideal filler for the preparation of composites with high thermal conductivity and electrical insulation. To obtain the expected enhancement in the thermal conductivity of composites, some researchers[32–34] specifically proposed an improved strategy based on the synergistic effect of BN and other fillers. In the strategy, BN was coated on the Al_2O_3 microspheres instead of a randomly dispersed hybrid of the two, thereby further enhancing the synergistic effect. Zou *et al.*[34] used a chemical coupling reaction to obtain BNNS-coated Al_2O_3 microspheres, and found that the thermal conductivity reached 2.43 W m^{-1} K^{-1} for the resulting EP composite with a filler content of 65 vol% and optimal BNNS-to-Al_2O_3 ratio of 1 : 7. This thermal conductivity value is significantly higher than that of the composites with only Al_2O_3 or the hybrid of Al_2O_3 and BN. However, such a high content of filler is not suitable for the preparation of the polyimide composite films.

In this work, on the basis of the several strategies referred above and our previous work,[35] a two-step synergism strategy was used for the first time to fabricate thermally conductive PI composite films containing BN nanoplatelets and Al_2O_3 microspheres. In the composite film, BN-coated modified Al_2O_3 (Al_2O_3@BN) was prepared by the electrostatic self-assembly method for the first step of synergism, and further collaborated with randomly oriented BN for the construction of a thermally conductive network with segregated structure for the second step of synergism. In the strategy, the ratio of the two fillers was optimized at a low content of 35 wt%, and the Al_2O_3@BN content was minimized to reduce the cost of materials, and the simple solution blending process was retained. Meanwhile, it is expected that the synergistic effect of BN and Al_2O_3 can be effectively exerted to obtain a relatively perfect three-dimensional thermally conductive network. The corresponding mechanism of heat conduction was also explored to provide a valuable reference for the design of novel conductive polymer composites.

2. Experimental

2.1. Materials

α-Al_2O_3 microspheres with an average particle size of 5 μm were supplied by Xiamen Zhanfan Trading Co., LTD., China. Hexagonal BN nanosheets, with a diameter of 0.5–1 μm and thickness of about 30 nm, were purchased from Shanghai Xiang Tian Nanomaterials Co., LTD., China. γ-Aminopropyl-triethoxysilane coupling agent (product name: KH550) and phthalic anhydride (PMDA) were provided by China Alighting Technology Co., LTD. 4,4-Diaminodiphenyl ether (ODA) was obtained from Shanghai Macklin Biochemical Technology Co., LTD., China. *N*,*N*-Dimethyl acetamide (DMAC), absolute ethyl alcohol and glacial acetic acid were purchased from Xilong Scientific Co., Ltd., China.

2.2. Fabrication of BN coated Al_2O_3 hybrid

As shown in Fig. 1, the preparation process of the BN coated Al_2O_3 hybrid (Al_2O_3@BN) included the following three parts: (1) surface functionalization of BN:[32,36] BN was subjected to heat treatment at 900 °C for 3 h, and ultrasonic treatment in deionized water for 5 h to obtain the hydroxylated BN (BN–OH) after drying in vacuum oven for 12 h. (2) Surface functionalization of Al_2O_3:[37] Al_2O_3 was added to a round-bottomed flask containing KH550 ethanol–water solution with a concentration of 2 wt% (pH 5–6 with glacial acetic acid for adjusting the pH value), and stirred mechanically for 2 h in a water bath at 60 °C. The resulting mixture was filtered, and the wet filter cake was washed with ethanol three times to remove the residual coupling agent. After drying overnight in a vacuum oven, the surface-aminated Al_2O_3 (Al_2O_3–KH550) was obtained. (3) Electrostatic self-assembly of Al_2O_3 and BN:[35] the weighted BN–OH and Al_2O_3–KH550 in a certain ratio were added to deionized water (pH 4–5 with glacial acetic acid for adjusting the pH value), and then ultrasonically dispersed for 30 min and further mildly stirred for 4 h. In this process, under an acidic condition, Al_2O_3–KH550 was positively charged due to surface amino hydrolysis, and BN–OH was negatively charged due to surface hydroxyl hydrolysis. The negatively charged BN and the positively charged Al_2O_3 were self-assembled under static electricity to realize the coating of BN on Al_2O_3. The final product Al_2O_3@BN was obtained by collecting and drying the precipitate of the suspension, achieving the first synergistic effect of the two fillers.

2.3. Preparation of PI composite films

Fig. 2 shows the synthesis route of the two-step preparation process of the PI film. A fixed filling of 35 wt% was selected for the preparation of the PI composite films, in which the 35 wt% filling for BN or Al_2O_3 generally exceeded the thermal percolation threshold and met the condition of forming the thermally conductive network.[6] As a representative PI composite film, the Al_2O_3@BN&BN/PI composite film was prepared, as shown in Fig. 1. To realize the second synergistic effect of Al_2O_3 and BN, 6.3 g hybrid of Al_2O_3@BN and BN in specific proportions was added in the solution of 8.615 g ODA and 82 g DMAC at room temperature, and then the mixture was mechanically stirred for 4 h. Subsequently, 9.385 g PMDA equivalent to ODA was added

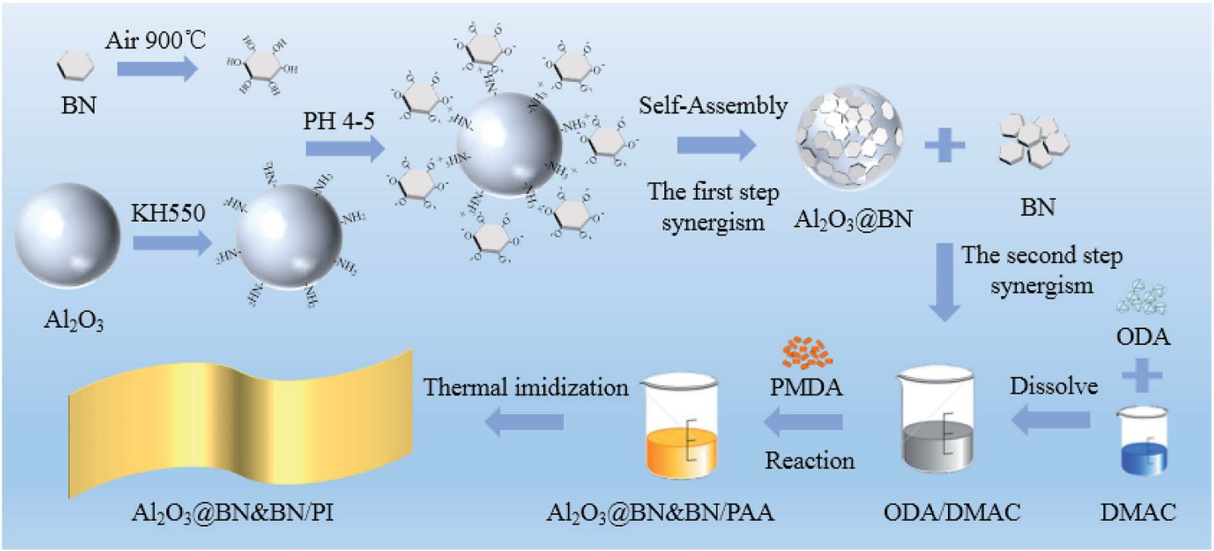

Fig. 1 Schematic illustration of Al_2O_3@BN preparation and fabrication process of the Al_2O_3@BN&BN/PI composite film.

to the mixture in batches within 2 h, followed by the continued reaction for 2 h. The obtained poly(amic acid) (PAA) composite solution was placed in a vacuum oven to remove bubbles. Finally, the solution was spread on a clean glass substrate, followed by thermal imidization in an oven from room temperature to 350 °C at a rate of 2 °C min^{-1} and at 350 °C for 1 h. The Al_2O_3@BN&BN/PI composite film with a thickness of around 80 μm was obtained from the glass substrate by immersion in hot water. For comparison, using a similar procedure, the pure PI film and the BN/PI, Al_2O_3/PI, Al_2O_3@BN/PI and Al_2O_3&BN/PI composite films were prepared by adding the different fillers, respectively. It should be noted that the Al_2O_3&BN/PI composite film was obtained by adding the two fillers at the same time.

2.4. Characterization

Scanning electron microscopy (SEM, Quanta FEG 450, FEI, USA) was used to investigate the surface morphology of the different fillers and the microstructure of the corresponding PI composite films. Fourier transform infrared spectroscopy (FTIR, TENSOR 27, BRUKER, Germany) was used to characterize the changes of the surface functional groups before and after modification of Al_2O_3 and BN. An energy dispersive X-ray spectrometer (EDS, X-MAX20, Oxford, UK) was used to analyze the distribution of elements B and Al in the composite film. A thermal conductivity analyzer (TPS2500S, HOT DISK, Sweden) was utilized to measure the in-plane thermal conductivity of pure PI and PI composite films, according to the transient plane source method testing standard (ISO 22007-2). The specimens were disk-like with a diameter of 20 mm and thickness of around 0.25 mm by stacking three layers of the films. Infrared thermography (FLIR, E50, Germany) was used to record changes in the surface temperature of the pure PI and PI composite films. Thermal gravimetric analysis (TGA, STA449F3, NETZSCH, Germany) was carried out to evaluate the thermal stability of the PI thermal composite films in the range from room temperature to 900 °C at 10 °C min^{-1} under the protection of nitrogen. A precision impedance analyzer (4294A, Agilent, USA) was used to analyze the dielectric properties of the pure PI and PI composite films at room temperature in the frequency range of 10^3 to 10^8 Hz. The specimens for the dielectric properties analysis were 1 cm thick, and pasted with aluminum foil on both sides. The tensile strength of the pure PI film and composite films was measured using a universal tensile tester (KDL5000N, KAIDE, China) at room temperature with a cross-head rate of 2 mm min^{-1}. The dumb-bell specimens (Type 5) were prepared in accordance with ISO 527-3.

3. Results and discussion

3.1. Characterizations of Al_2O_3@BN

Fig. 3a shows that the morphology of Al_2O_3 was typically spherical with a relatively smooth surface, and had a diameter

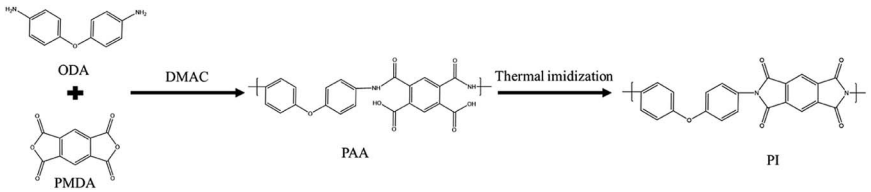

Fig. 2 Synthesis route of the pure PI.

in the range of 1–8 μm and a wide particle size distribution. Fig. 3b shows that the shape of the BN was typically flaky with a size of 500 nm–1 μm. As shown in Fig. 3c–g, the morphology of Al_2O_3@BN was significantly changed compared to that of Al_2O_3 in Fig. 3a. A certain amount of flaky BN particles were evenly coated on the surface of Al_2O_3, and the amount of BN on the surface of Al_2O_3 accordingly decreased with the increase of the mass ratio of Al_2O_3 to BN. On the whole, this indicates that the coating of Al_2O_3 by BN was successfully realized by using the principle of electrostatic self-assembly, and the coating amount of BN can be controlled by changing the mass ratio of the two fillers. However, Fig. 3c shows that BN did not completely coat the surface of Al_2O_3, which may be due to the small amount of KH550 that caused the charges on the surface of Al_2O_3 to be insufficient to attract enough BN. At the same time, it can be clearly seen that BN was scattered around the Al_2O_3 particles. This is mainly attributed to the fact that the total amount of BN exceeded the limit of charge balance between BN and Al_2O_3, and the excess BN cannot be attracted to the surface of Al_2O_3. In addition, a small amount of BN coated on Al_2O_3 was detached from Al_2O_3 during the sample preparation process due to the weak interaction between BN and Al_2O_3. This finding is a common phenomenon in the preparation of composite particles by electrostatic self-assembly.[36] Zou *et al.*[34] reported that the chemical bonding between BNNS and Al_2O_3 was introduced to obtain a better and stable coating in Al_2O_3@BNNS. However, the corresponding preparation process was more complicated than the electrostatic self-assembly method. As far as the preparation process in this work is concerned, 2 : 1 was optimized among the different proportions of Al_2O_3 to BN. As shown in Fig. 3d, the resulting Al_2O_3@BN had a relatively high coating amount similar to that in the proportion of 1 : 1 (Fig. 3c), and BN was almost not excessive.

In order to clearly observe whether BN is uniformly coated on the surface of Al_2O_3, the magnified SEM images of Al_2O_3@BN with different particle sizes of Al_2O_3 at 2 : 1 mass ratio of Al_2O_3 to BN is shown in Fig. 3h and i. It is clear that the particle size of Al_2O_3 has an effect on the amount of BN coating. The amount of BN coated on Al_2O_3 with smaller particle size is less than that with larger particle size, which may be attributed to the steric hindrance of BN on the surface of Al_2O_3 with small particle size. Although BN did not completely coat the surface of Al_2O_3, the distribution of BN on the surface of Al_2O_3 was uniform and independent of particle size.

Fig. 4a gives the FTIR spectra of BN before and after hydroxyl modification. The two strong absorption peaks at 1384 cm^{-1} and 807 cm^{-1} are attributed to the in-plane tensile vibration and out-of-plane bending vibration of B–N,[36,37] respectively. The modified BN shows a hydroxyl absorption peak at 3230 cm^{-1} that is wider and stronger than that of the original BN, indicating the successful hydroxyl modification of BN.[32,37] Fig. 4b shows the FTIR spectra of pristine Al_2O_3, Al_2O_3–KH550 and

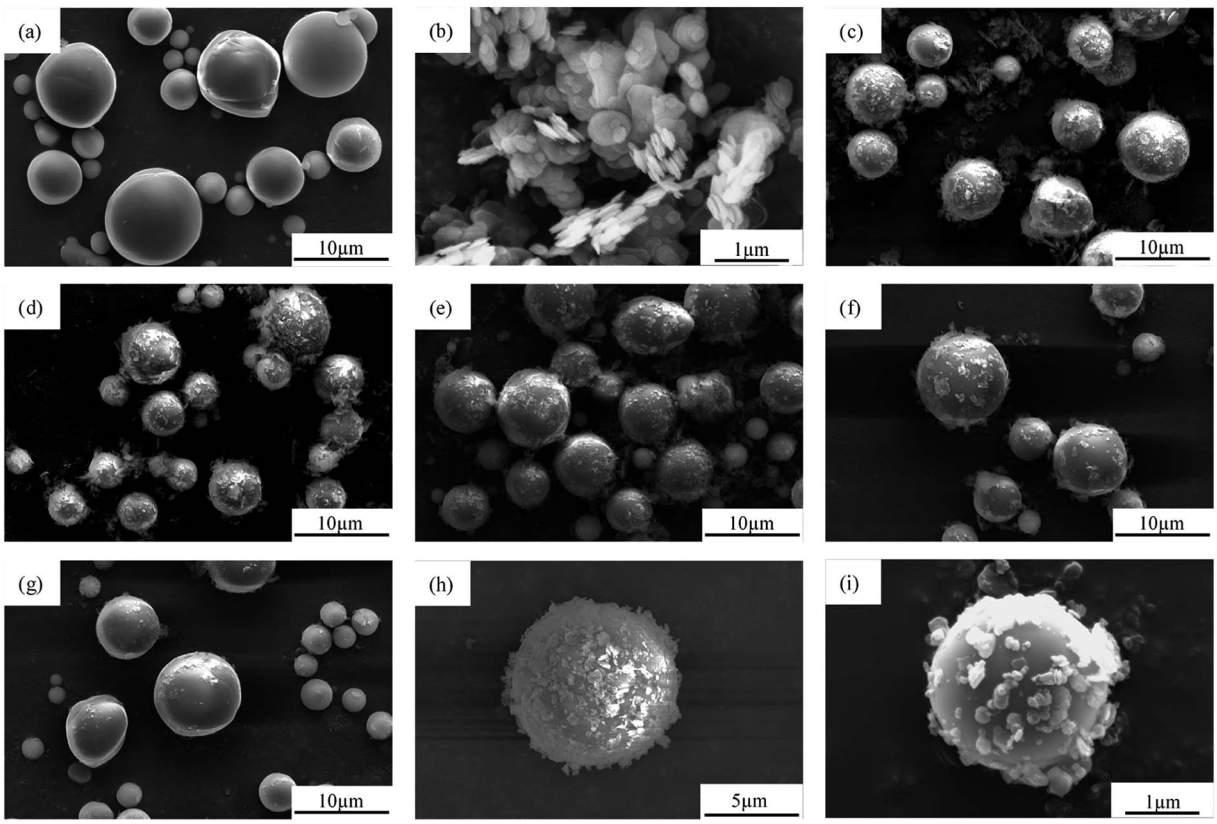

Fig. 3 SEM images of (a) Al_2O_3, (b) BN and (c–i) Al_2O_3@BN with different ratios of Al_2O_3 to BN: (c) 1 : 1, (d, h and i) 2 : 1, (e) 3 : 1, (f) 4 : 1 and (g) 5 : 1.

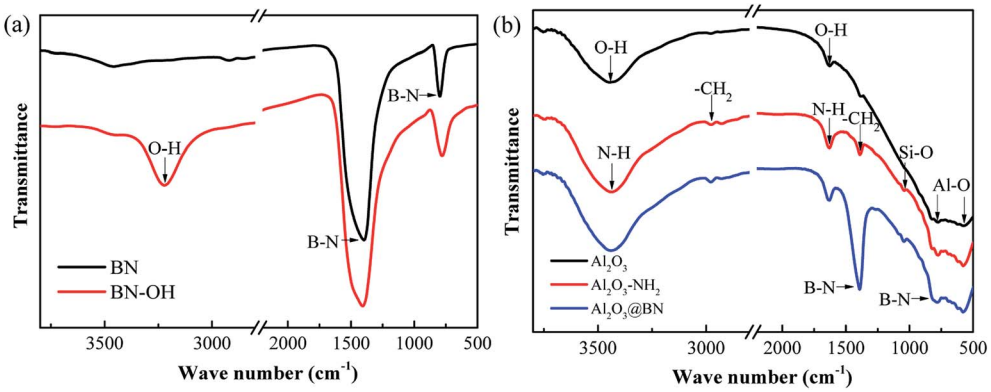

Fig. 4 FTIR spectra of (a) BN and BN–OH, (b) Al_2O_3, Al_2O_3–NH_2 and Al_2O_3@BN.

Al_2O_3@BN. The absorption peaks at 763 cm^{-1} and 567 cm^{-1} corresponding to Al–O were observed from all samples, and the absorption peaks at 3434 cm^{-1} and 1647 cm^{-1} are attributed to the stretching and bending of –OH, respectively.[38,39] After functionalization of Al_2O_3 with KH550, a new Si–O absorption peak appeared at 1046 cm^{-1}, and the stretching and bending absorption peaks of N–H were observed at 3441 cm^{-1} and 1631 cm^{-1}, respectively. In addition, the absorption peaks at 2980 cm^{-1} and 1388 cm^{-1} are characteristic of the asymmetric and symmetric stretching vibrations of $-CH_2$, respectively. These results indicate that Al_2O_3 was successfully modified with KH550 in the form of a covalent bond, and the amino groups were introduced onto the surface of Al_2O_3.[37,38] The B–N characteristic peaks from Al_2O_3@BN at 1386 cm^{-1} and 801 cm^{-1} further indirectly confirmed the successful coating of Al_2O_3 by BN.

3.2. Microstructure of PI composite films

SEM images of the teared fracture surface of the PI composite films with different fillers are shown in Fig. 5. The pure PI film (Fig. 5a) had a dense interior structure and a smooth fracture surface. As shown in Fig. 5b, although Al_2O_3 was uniformly distributed in the matrix of the Al_2O_3/PI composite film, there were obvious gaps between Al_2O_3 and the matrix, indicating a weak interface interaction and a high interfacial thermal resistance between them. For the BN/PI composite film (Fig. 5c), BN was relatively uniformly distributed in the matrix, but mainly in the form of thick layered aggregates, which means that a certain thermally conductive network was constructed.

When Al_2O_3 and BN were introduced together into the matrix (Fig. 5d), Al_2O_3 segregated the matrix into a continuous phase region, and BN was distributed in the matrix, which was a typical segregated structure. In contrast to that of the BN/PI composite film, the distribution state of BN in the matrix of the Al_2O_3&BN/PI composite film was changed by the segregated structure,[35] which is beneficial to the formation of a relatively perfect thermally conductive network in a low BN content. However, in the Al_2O_3&BN/PI composite film, the segregated structure was relatively sparse due to the large size and the limited loading of the Al_2O_3 microparticles. On the other hand, there was no effective contact between Al_2O_3 and the segregated BN network, which does not help to form an efficient thermally conductive network in the composite film. We also noted that the stacking or assembly of BN nanoparticles on the surface of the Al_2O_3 microparticles with no coupling agent treatment has already been reported in the literature,[32,37] in which the osmotic pressure difference between BN and Al_2O_3 in blending drives BN to stack on the surface of Al_2O_3. To achieve this, a very high alumina content (70 vol%) is required. However, the total content of the fillers is only 35 wt% in the Al_2O_3&BN/PI composite film, where the gap between the Al_2O_3 particles and between Al_2O_3 and BN is too large to produce enough osmotic pressure difference to drive BN to stack on the surface of alumina. In this work, BN should be successfully assembled on the surface of Al_2O_3 under the action of static electricity by the two-step method without the limitation of high filler loading.

Compared to that in the Al_2O_3/PI, the gaps between Al_2O_3 and the matrix in the Al_2O_3@BN/PI composite film (Fig. 5e) significantly decreased. Al_2O_3 was embedded in the matrix, which is helpful to reduce the interfacial contact thermal resistance between them. This change is mainly attributed to the coating of Al_2O_3 by BN, which can improve the wettability of Al_2O_3 by way of the PAA solution as a result of the similar interfacial chemistry between PI and BN.[40] Moreover, the surface modification of Al_2O_3 with KH550 can improve the interfacial interaction between PI and Al_2O_3, which can further reduce the interfacial contact thermal resistance between them. It can be further observed that there was the obvious BN in the matrix close to Al_2O_3, which should correspond to the BN detached from Al_2O_3 during the preparation of the composite film. Although Al_2O_3@BN also formed a certain segregated structure network in the PI matrix, the network was not perfect due to a low content of the detached BN. So, the large PI region (circled by yellow solid lines in Fig. 5e) appeared to hinder the formation of an effective thermally conductive network of BN. As shown in Fig. 5f, when BN and Al_2O_3@BN were used together in a certain proportion, a thermally conductive network of BN with segregated structure by Al_2O_3@BN in the Al_2O_3@BN&BN/PI composite film was obtained. This thermally conductive network was also denser and more complete compared to that in Al_2O_3&BN/PI. It can be seen that the fracture morphology of

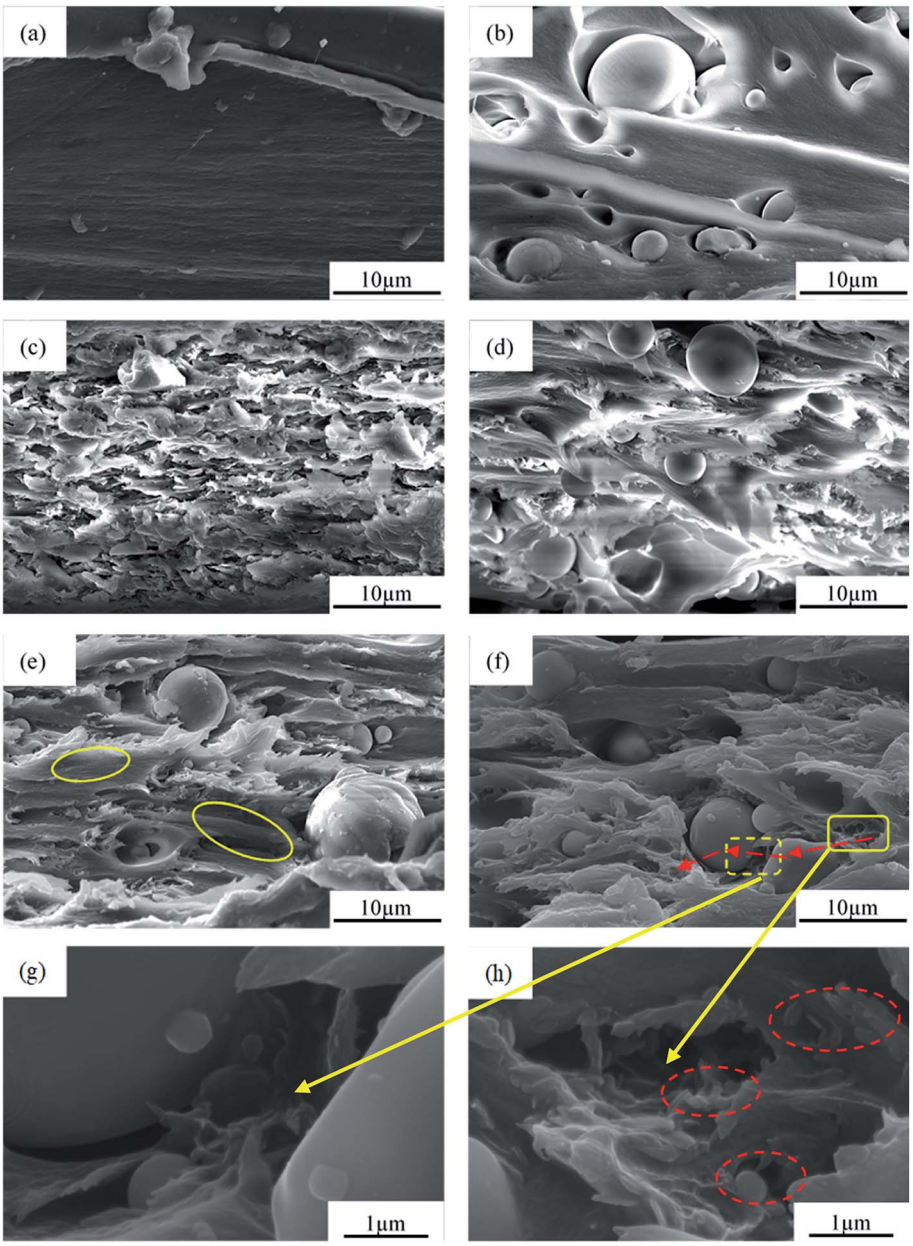

Fig. 5 SEM images of the teared fracture surface of the pure PI (a) and PI composites with different fillers: (b) Al_2O_3/PI, (c) BN/PI, (d) Al_2O_3&BN/PI, (e) Al_2O_3@BN/PI and (f–h) Al_2O_3@BN&BN/PI. The mass ratio of Al_2O_3 : BN is 2 : 1 in the composites (d–h).

the continual matrix around these Al_2O_3 particles was relatively rough compared to that without BN in Fig. 5b. In addition, there were no obvious layered agglomerations of BN in the matrix, which implies that BN was dispersed well in the matrix, and a denser thermally conductive network was constructed.

Fig. 5g shows the local magnification of the edge region (indicated by yellow dashed frame) of the Al_2O_3 microparticles in Fig. 5f. It can be found that BN was coated on the surface of Al_2O_3. This improved the interface adhesion between Al_2O_3 and the matrix, and reduced the interface thermal resistance. This also implies that the first step synergism of the two fillers was achieved. Meanwhile, the BN coating is also conducive to the contact between Al_2O_3 and the BN thermally conductive network in the matrix, playing a bridging role and participating in the construction of a relatively perfect thermally conductive network. Fig. 5h shows the further enlargement of the matrix zone close to Al_2O_3, which is surrounded by the yellow solid frame in Fig. 5f, and reveals that the BN in the matrix apparently formed a thermally conductive network. The red arrow in Fig. 5f indicates the efficient conductive path of heat flow in the composite film. The heat flow can be conducted along the paths *via* segregated BN thermally conductive network, Al_2O_3 and BN coated on the surface of Al_2O_3, indicating the second step synergism of the two fillers.

Fig. 6a shows the EDS element mapping on the same region, which corresponds to the Al_2O_3@BN&BN/PI composite film in

Fig. 5f. The distribution of element Al was consistent with the shape and distribution of Al_2O_3. Element B was relatively uniformly distributed in the matrix, which also indicates that BN constructed a dense thermally conductive network in the PI matrix. At the same time, element B also appeared in the position of Al_2O_3, suggesting that BN was coated on the surface of Al_2O_3. Additionally, element B was uniformly distributed in the edge region of Al_2O_3, where the distribution of element B overlapped with that of element Al. This implies that BN was in contact with the Al_2O_3 particles, playing a bridging role.

Based on the results of the EDS analysis and the SEM analysis above, Fig. 6b gives a schematic diagram of the heat transfer mechanism of the Al_2O_3@BN&BN/PI composite film. Al_2O_3 and BN synergistically construct an efficient thermally conductive network in the composite film in a two-step process. The Al_2O_3@BN with the first synergistic effect segregates the PI matrix, so that the BN dispersed in the matrix forms a thermally conductive network with a segregated structure. The effective contact between Al_2O_3 and BN further enhances the thermally conductive network *via* the bridging effect of the BN coated on Al_2O_3, achieving the second step synergism of the two fillers. When the heat flow is conducted in the in-plane direction, it can be transferred efficiently from high temperature to low temperature along the path *via* the BN-segregated thermally conductive network, the BN coated on the surface of Al_2O_3 and Al_2O_3. In summary, several strategies were used to enhance the thermal conductivity of the Al_2O_3@BN&BN/PI composite film, which mainly include: (1) the synergism of the fillers hybrid, (2) the construction of a three-dimensional segregated network, (3) the strengthening of a thermally conductive interface, and (4) the network bridging. Among them, the coating of BN on the surface of Al_2O_3 by electrostatic self-assembly played a key role in building a perfect heat conduction network by bridging the heat conduction network.

3.3. Thermal conductivity of PI composite films

Fig. 7a and b show the in-plane thermal conductivity of the different PI composites with different mass ratios of Al_2O_3 to BN at a total filler content of 35 wt%, and the corresponding thermal conductivity enhancement compared to pure PI, respectively. The thermal conductivity of the Al_2O_3/PI composite film increased to 2.45 W m^{-1} K^{-1}, and was 1189% higher than that of pure PI (0.19 W m^{-1} K^{-1}), which indicates that the Al_2O_3 loading of 35 wt% exceeds the thermal conductivity percolation threshold. The addition of Al_2O_3 can also significantly improve the thermal conductivity of the PI composite film. On the other hand, although the inherent thermal conductivity of BN is significantly higher than that of Al_2O_3, the thermal conductivity of the BN/PI composite film (2.73 W m^{-1} K^{-1}) was only slightly higher than that of the Al_2O_3/PI composite film. As illustrated by Fig. 5c, these results are mainly attributed to the agglomeration and layered distribution of BN, which are not conducive to the formation of an effective thermal conduction network. By the introduction of BN in all mass ratios of Al_2O_3 to BN, the thermal conductivity of the Al_2O_3&BN/PI composite films was further enhanced compared to that of the Al_2O_3/PI composite film, but was not higher than that of the BN/PI composite film. Apparently, Al_2O_3 and BN cannot play a significantly synergistic effect in a random hybrid form, despite constructing the expected segregated structure. This is mainly attributed to no bridging between the Al_2O_3 and the BN thermally conductive network, and the poor wettability of Al_2O_3 to the PI matrix.

For the Al_2O_3@BN/PI composite films, the thermal conductivity changed significantly with the variety of the mass ratio of Al_2O_3 to BN. The mass ratio of Al_2O_3 to BN of 2 : 1 was optimized for the improvement of the thermal conductivity. The thermal conductivity of the resulting composite film was increased to 2.74 W m^{-1} K^{-1} and even slightly higher than that of the BN/PI composite film, indicating the first synergistic effect of Al_2O_3 and BN. Referring to the SEM analysis, this result is attributed to the fact that the coating of Al_2O_3 by BN can increase the interfacial compatibility between Al_2O_3 and the PI matrix, and accordingly reduce the interfacial thermal resistance. Moreover, part of the BN detached from Al_2O_3 was dispersed in the PI matrix, and a certain thermally conductive network with segregated structure was constructed.

When BN was further used together with Al_2O_3@BN in the different ratios, as the result of the two-step synergism, the thermal conductivity of the Al_2O_3@BN&BN/PI composite films was significantly improved compared to that of the Al_2O_3@BN/PI composite films. It was also higher than that of the BN/PI composite film. When the mass ratio of Al_2O_3@BN to BN was 2 : 1, the thermal conductivity of the Al_2O_3@BN&BN/PI composite film was increased to the highest value of 3.35 W m^{-1} K^{-1}, and was 1664% higher than that of pure PI. It was also 36.6%, 23%, 22% and 28.4% higher than the Al_2O_3/PI, BN/PI, Al_2O_3@BN/PI and Al_2O_3&BN/PI composite films, respectively. This indicates that the two-step synergistic effect of Al_2O_3 and

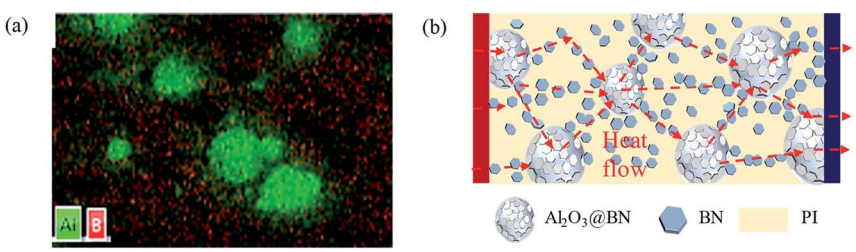

Fig. 6 (a) EDS element mapping of the Al_2O_3@BN&BN/PI composites. (b) Schematic diagram of the heat transfer in the Al_2O_3@BN&BN/PI composites.

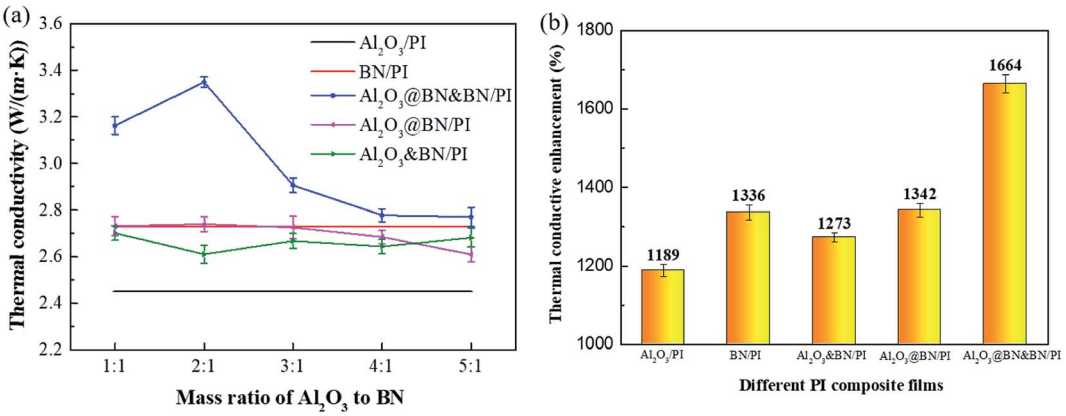

Fig. 7 (a) Thermal conductivity of the PI composite film with different mass ratios of Al_2O_3 to BN. (b) Thermal conductivity enhancement of different PI composite films with the Al_2O_3-to-BN mass ratio of 2 : 1.

BN at the mass ratio of 2 : 1 is the most significant in the Al_2O_3@BN&BN/PI composite film. In contrast, the thermal conductivity of the Al_2O_3@BN&BN/PI composite films with other ratios of Al_2O_3@BN to BN was decreased. For the ratio of 1 : 1, a low Al_2O_3 content is not conducive to the construction of the segregated structure. When the ratio was higher than 3 : 1, the low-content BN cannot form the complete thermally conductive network, resulting in the decrease of the thermal conductivity with the increase of the ratio.

Fig. 8 exhibits the evaluation of the potential application of the PI composites for the thermal management of the electronic product. As shown in Fig. 8a and b, the as-prepared composite films were used as substrates to support a light emitting diode (LED) chip using thermal grease. The variations of the maximum surface temperature of the LED chip as a heat source were measured in a timely manner by a portable infrared thermal imager (Fig. 8c and d). The temperature rise and equilibrium temperature of the LED chip with working time reflect the differences in the heat conduction and heat dissipation of the PI composite films, which is consistent with those in the corresponding thermal conductivity in Fig. 7. Under the same LED working conditions, the Al_2O_3@BN&BN/PI composite film displayed a relatively lower temperature rise rate and a significantly lower equilibrium temperature than those of the other composite films. For example, the corresponding equilibrium temperature was about 81 °C, and 26.1 °C lower than that of the pure PI film, reflecting the good heat conduction and heat dissipation of the Al_2O_3@BN&BN/PI composite film.

To assess the enhancement of the thermal conductivity of the Al_2O_3@BN&BN/PI composite films, a comparison on the thermal conductivity of the relevant PI thermal conductivity composite films reported in the last year is given in Table 1. The thermally conductive fillers used in the PI composite films involved several common electrically conductive fillers, such as Cu, Ag and graphene, and the insulating thermal conductive fillers, such as BN, Al_2O_3, SiC and AlN. The nano-sized fillers, especially for metal or carbon nanomaterials with excellent thermal conductivity, can generally achieve significant enhancement at a low filling (<15 wt%). It is noteworthy that only 7 wt% BNNS fabricated by the efficient exfoliation of BN nanosheets increased the thermal conductivity by 1080%,[14] which is similar to the enhancing effect of the conventional BN of more than 30 wt%. Apparently, great attention has been paid to the synergism of the fillers hybrid for further improvement of the thermal conductivity. The graphene woven fibers prepared by template method have also achieved the significant enhancement of 1418% only at 11 wt% content due to the construction of an efficient three-dimensional network. In the practical application, considering the economy and process simplicity, the >30 wt% micro-sized BN,[41,42] Al_2O_3 (ref. 31) and AlN[31] were commonly introduced to the PI matrix to achieve an increase of 1000% in the thermal conductivity, while also meeting a practical requirement of heat management.[43] By comparison, the 35 wt% Al_2O_3@BN&BN/PI composite film containing 17 wt% BN and 18 wt% Al_2O_3 achieved the thermal conductivity of 3.35 W m^{-1} K^{-1} and a relatively high enhancement of 1664%. This means that the strategy of the two-step synergism used in this work had a significant effect in improving the thermal conductivity of the PI composite film. Moreover, the combination of Al_2O_3 and BN can reduce the cost of fillers and retain the advantages of process simplicity.

3.4. Thermal stability of PI composite films

The thermal stability of the pure PI and PI composite films was evaluated by TGA, and the main thermal parameters of different prepared PI composite films are shown in Table 2. Clearly, the pure PI and all kinds of PI composites exhibited excellent thermal stability, which is mainly attributed to the presence of aniline and imide rings in the polyimide molecular chains.[6] For example, the thermal stability temperatures of the pure PI corresponding to 5% weight loss ($T_{5\%}$), 10% weight loss ($T_{10\%}$) and the maximum degradation rate (T_{max}), occurred at 562.8 °C, 576.9 °C and 591.1 °C, respectively. The thermal stability of all PI composite films has been improved to some extent because both BN and Al_2O_3 have a high heat capacity and thermal conductivity, and play a role of mass transfer barriers to inhibit the escape of volatile degradants.[6,16]

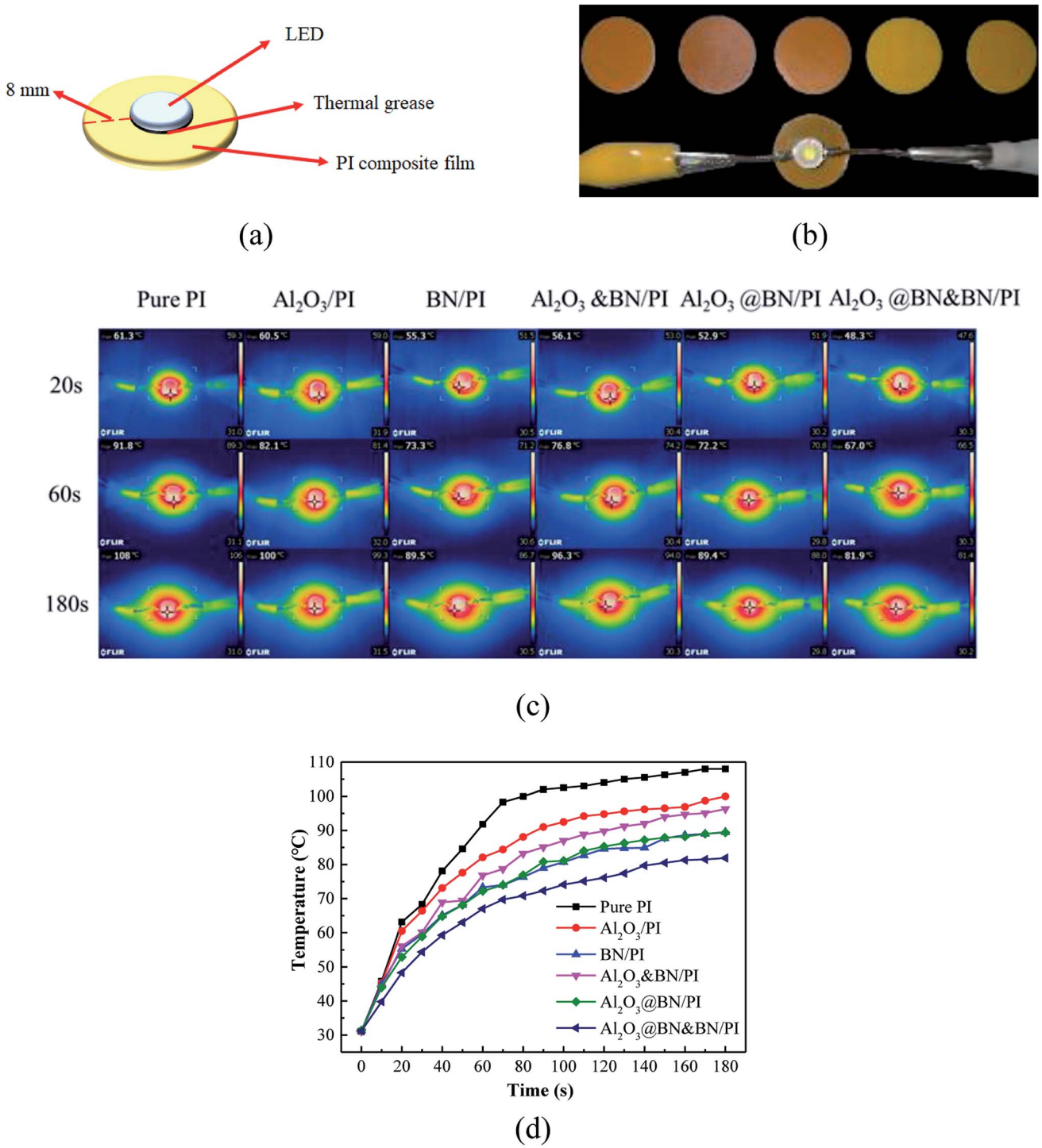

Fig. 8 Evaluation of the potential application of the PI composites for thermal management of electronic products: (a) schematic diagram of the PI composite film supporting the LED module, (b) photos of different PI composites, (c) infrared thermal imaging of LED with different PI composite substrates varying with working time, and (d) the surface temperature of LED with different PI composite substrates as a function of the working time.

3.5. Dielectric properties of PI composite films

Fig. 9 shows the variation of the dielectric constant and dielectric loss with frequency for the pure PI and the PI composite films with the different fillers. The relative permittivity and the dielectric loss of pure PI at 1 kHz were 1.8 and 0.007, respectively. The introduction of BN and Al_2O_3 increased the permittivity and dielectric loss to some extent due to the interfacial polarization effect of the fillers. Because the specific surface area of the flake BN is larger than that of Al_2O_3 and the interfacial polarization effect produced by BN is greater than

Table 1 A comparison of various fillers for the in-plane thermal conductivity enhancement of PI composite films

Filler	Content (wt%)	λ (W m^{-1} K^{-1})	Enhancement (%)	Ref.
BN layer coated Cu nanowires	10	2.61	1417	29
Ag nanoparticles loaded rGO	15	2.12	685	7
Graphene woven fibers	12	3.73	1418	30
SiC nanowires grafted graphene	11	2.63	989	10
Al_2O_3	30	2.41	980	31
AlN	30	2.40	980	
BN	30	2.81	1320	6
Exfoliated BN nanosheet	7	2.95	1080	14
Al_2O_3@BN&BN	35	3.35	1664	This work

Table 2 Characteristic thermal data of the PI composite films with different fillers

Sample	$T_{5\%}$ (°C)	$T_{10\%}$ (°C)	T_{max} (°C)	Residual at 900 °C (%)
Pure PI	562.8	576.9	591.1	56.21
Al_2O_3/PI	563.4	581.8	591.4	67.98
BN/PI	567.9	591.8	606.4	64.69
Al_2O_3&BN/PI	562.9	578.6	602.1	67.76
Al_2O_3@BNPI	565.2	581.2	595.7	65.18
Al_2O_3@BN&BN/PI	563.3	579.9	597.3	69.39

that of Al_2O_3,[44] the permittivity and dielectric loss of the BN/PI composite film were higher than those of the Al_2O_3/PI composite film. The relative permittivity and the dielectric loss of the Al_2O_3@BN&BN/PI composite films at 1 kHz were 2.48 and 0.013, respectively, which are low values for the dielectric properties of the thermally conductive composite and suitable for insulated electronic packaging applications.

3.6. Mechanical properties of PI composite films

The mechanical properties of the filled polymer composites are of great significance in practical applications, but are generally deteriorated due to serious agglomeration under high filling content.[45,46] The tensile test of the PI film and PI composite films was conducted to investigate the tensile strength of different composite films, and evaluated the flexibility of the Al_2O_3@BN&BN/PI composite film. As shown in Fig. 10a, the Al_2O_3@BN&BN/PI composite film was folded easily and was not broken after being folded many times, indicating its good flexibility. Fig. 10b shows the variety of tensile strengths of different composite films. The tensile strength of the pure PI composite films is 90.4 MPa. The tensile strength of the composite films was decreased to some extent due to the stress concentration from the high-loading fillers. The tensile strength of the BN/PI composite film was the lowest and decreased by 74.4% compared to that of the pure PI film, which should be attributed to the layered agglomeration of BN. According to the SEM analysis above, micron-sized spherical Al_2O_3 was easily dispersed in the matrix. The addition of Al_2O_3 also changed the distribution of the fillers, resulting in a reduction of the stress concentration. Therefore, the tensile strength of the composite films containing Al_2O_3 did not seriously deteriorate. The tensile strength of Al_2O_3/PI, Al_2O_3&BN/PI and Al_2O_3@BN/PI was decreased by 29.8%, 28.5% and 28.6%, respectively. The Al_2O_3@BN&BN/PI composite film had the highest tensile strength among all composite films. This means that the Al_2O_3@BN&BN/PI composite film was significantly improved in thermal conductivity by the two-step synergism of the fillers, while its mechanical properties were maintained.

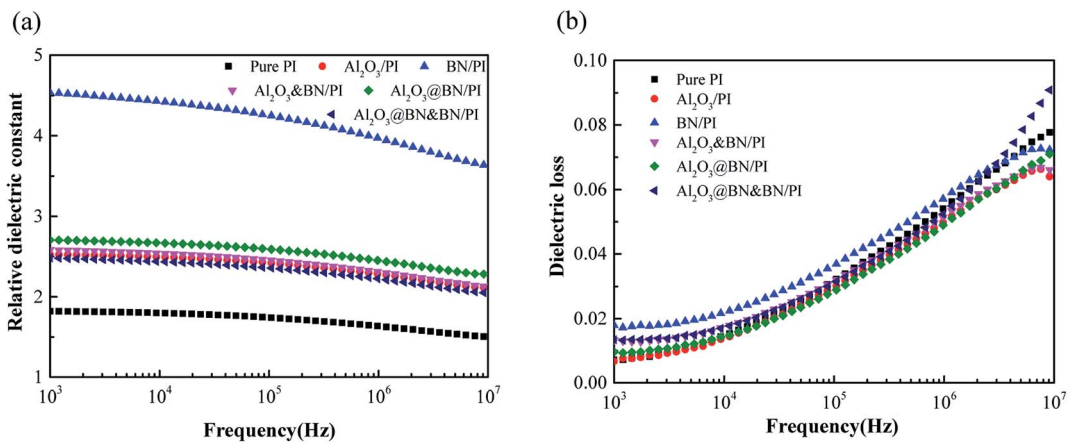

Fig. 9 Frequency dependence of (a) the dielectric constant and (b) dielectric loss of the PI composites with different fillers.

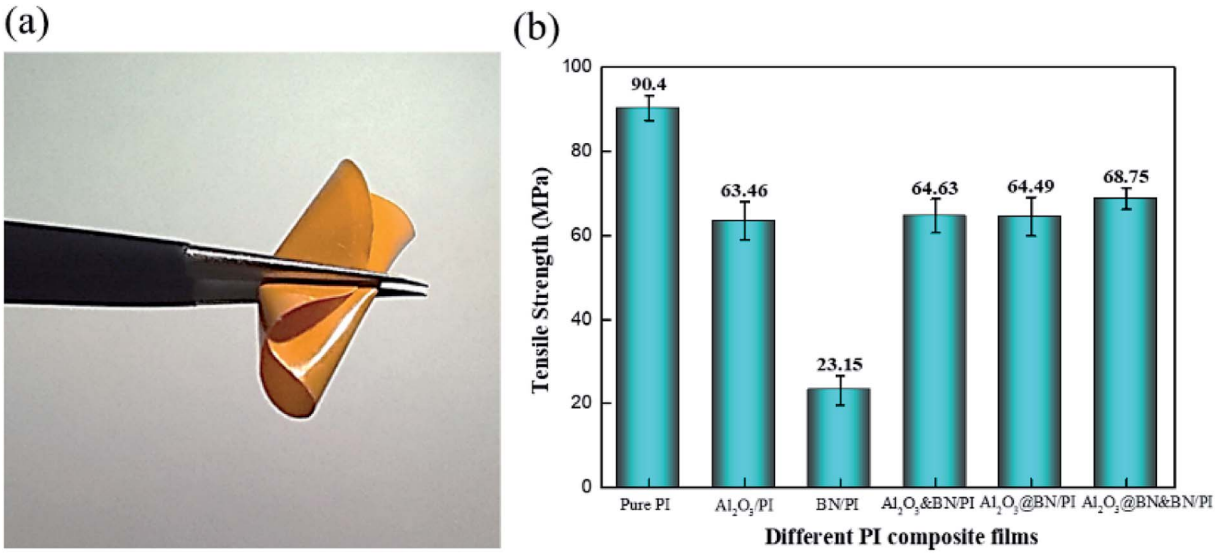

Fig. 10 (a) A digital image of the folded Al_2O_3@BN&BN/PI film, and (b) the tensile strength of the pure PI and composite films.

4. Conclusions

In this work, a strategy of two-step synergism was proposed to significantly improve the thermal conductivity of PI films with respect to the efficient construction of a three-dimensional conductive network, and to the economy and simplicity of processing. For the first step of the synergism, BN-coated modified Al_2O_3 composite particles (Al_2O_3@BN) were successfully prepared by the electrostatic self-assembly method. The BN coated on the surface of Al_2O_3 played the roles of bridging the thermally conductive network, and improving the interface between Al_2O_3 and PI. For the second step of the synergism, Al_2O_3@BN further collaborated with BN to fabricate the Al_2O_3@BN&BN/PI composite film, in which Al_2O_3 helped BN to form a thermally conductive network with a segregated structure in the PI matrix. Accordingly, under the two-step synergistic effect of the two fillers, the thermal conductivity of the Al_2O_3@BN&BN/PI composite film was significantly improved compared to that of pure PI and the other control composite films. The Al_2O_3-to-BN mass ratio of 2 : 1 was optimum for preparing the Al_2O_3@BN&BN/PI composite film. When the mass ratio of Al_2O_3@BN to BN was 2 : 1, the thermal conductivity of the PI composite film with the filler content of 35 wt% increased to the maximum value of 3.35 W m^{-1} K^{-1}, which was 1664% higher than that of pure PI. Compared with the relevant studies, this is a high-level enhancement effect. In addition, the composite film had excellent dielectric properties, thermal stability and mechanical properties, which is expected to have potential applications in the fields of electronic packaging materials, thermal management materials and thermal interface materials. The strategy of the two-step synergism of fillers for the enhancement of the Al_2O_3@BN&BN/PI composite film is also recommended for the design and preparation of novel polymer composites with high thermal conductivity or electrical conductivity.

Conflicts of interest

The authors declare that they have no known competing financial interests or personal relationships that could have appeared to influence the work reported in this paper.

Acknowledgements

The authors are grateful to the National Natural Science Foundation of China (51763006), the Science and Technology Major Project of Guangxi Province (AA18242010-2), the Graduate Education Innovation Program Project of Guangxi Province (YCSW2020161), and the Natural Science Foundation of Guangxi Province (2019GXNSFGA245005) for financial support for this work.

References

1 H. Chen, V. V. Ginzburg, J. Yang, Y. Yang, W. Liu, Y. Huang, L. Du and B. Chen, *Prog. Polym. Sci.*, 2016, **59**, 41–85.
2 Z. A. Qureshi, H. M. Ali and S. Khushnood, *Int. J. Heat Mass Transfer*, 2018, **127**, 838–856.
3 W. Feng, M. Qin and Y. Feng, *Carbon*, 2016, **109**, 575–597.
4 J. Kim, J. Kwon, D. Lee, M. Kim and H. Han, *Korean J. Chem. Eng.*, 2016, **33**, 3245–3250.
5 J. W. Xia, G. P. Zhang, L. Deng, H. P. Yang, R. Sun and C. P. Wong, *RSC Adv.*, 2015, **5**, 19315–19320.
6 H. Wang, D. Ding, Q. Liu, Y. Chen and Q. Zhang, *Composites, Part B*, 2019, **158**, 311–318.
7 Y. Guo, X. Yang, K. Ruan, J. Kong, M. Dong, J. Zhang, J. Gu and Z. Guo, *ACS Appl. Mater. Interfaces*, 2019, **11**, 25465–25473.
8 S. Wei, Q. Yu, Z. Fan, S. Liu, Z. Chi, X. Chen, Y. Zhang and J. Xu, *RSC Adv.*, 2018, **8**, 22169–22176.
9 S. Uchida, R. Ishige and S. Ando, *Polymers*, 2017, **9**, 263–273.

10 W. Dai, J. Yu, Y. Wang, Y. Song, F. E. Alam, K. Nishimura, C.-T. Lin and N. Jiang, *J. Mater. Chem. A*, 2015, **3**, 4884–4891.
11 Z. Han and A. Fina, *Prog. Polym. Sci.*, 2011, **36**, 914–944.
12 J. Yang, L. Tang, L. Bai, R. Bao, Z. Liu, B. Xie, M.-B. Yang and W. Yang, *Mater. Horiz.*, 2019, **6**, 250–273.
13 N. Song, S. Cui, D. Jiao, X. Hou, P. Ding and L. Shi, *Carbon*, 2017, **115**, 338–346.
14 T. Wang, M. Wang, L. Fu, Z. Duan, Y. Chen, X. Hou, Y. Wu, S. Li, L. Guo, R. Kang, N. Jiang and J. Yu, *Sci. Rep.*, 2018, **8**, 1557.
15 X. Zeng, J. Sun, Y. Yao, R. Sun, J. B. Xu and C. P. Wong, *ACS Nano*, 2017, **11**, 5167–5178.
16 Y. Guo, Z. Lyu, X. Yang, Y. Lu, K. Ruan, Y. Wu, J. Kong and J. Gu, *Composites, Part B*, 2019, **164**, 732–739.
17 M. Qin, Y. Feng, T. Ji and W. Feng, *Carbon*, 2016, **104**, 157–168.
18 M. Qin, Y. Xu, R. Cao, W. Feng and L. Chen, *Adv. Funct. Mater.*, 2018, **28**, 1805053–1805065.
19 Z. Tian, J. Sun, S. Wang, X. Zeng, S. Zhou, S. Bai, N. Zhao and C.-P. Wong, *J. Mater. Chem. A*, 2018, **6**, 17540–17547.
20 Y. Yao, X. Zhu, X. Zeng, R. Sun, J.-B. Xu and C.-P. Wong, *ACS Appl. Mater. Interfaces*, 2018, **10**, 9669–9678.
21 J. Hu, Y. Huang, Y. Yao, G. Pan, J. Sun, X. Zeng, R. Sun, J. B. Xu, B. Song and C. P. Wong, *ACS Appl. Mater. Interfaces*, 2017, **9**, 13544–13553.
22 B. Liu, Y. Li, T. Fei, S. Han, C. Xia, Z. Shan and J. Jiang, *Chem. Eng. J.*, 2020, **385**, 123829–123841.
23 Y. Zhou, S. Wu and F. Liu, *Mater. Lett.*, 2019, **237**, 19–21.
24 W. Dai, L. Lv, J. Lu, H. Hou, Q. Yan, F. E. Alam, Y. Li, X. Zeng, J. Yu, Q. Wei, X. Xu, J. Wu, N. Jiang, S. Du, R. Sun, J. Xu, C. P. Wong and C. T. Lin, *ACS Nano*, 2019, **13**, 1547–1554.
25 W. Zhao, J. Kong, H. Liu, Q. Zhuang, J. Gu and Z. Guo, *Nanoscale*, 2016, **8**, 19984–19993.
26 J. Han, G. Du, W. Gao and H. Bai, *Adv. Funct. Mater.*, 2019, **29**, 1900412–1900421.
27 N. Sun, J. Sun, X. Zeng, P. Chen, J. Qian, R. Xia and R. Sun, *Composites, Part A*, 2018, **110**, 45–52.
28 X. Wu, H. Li, K. Cheng, H. Qiu and J. Yang, *Nanoscale*, 2019, **11**, 8219–8225.
29 Y. Zhou, S. Yu, H. Niu and F. Liu, *Polymers*, 2018, **10**, 1412–1419.
30 J. Gong, Z. Liu, J. Yu, D. Dai, W. Dai, S. Du, C. Li, N. Jiang, Z. Zhan and C. Lin, *Composites, Part A*, 2016, **87**, 290–296.
31 H. Song, B. G. Kim, Y. S. Kim, Y. S. Bae, J. Kim and Y. Yoo, *Polymers*, 2019, **11**, 484–493.
32 Y.-K. Kim, J.-Y. Chung, J.-G. Lee, Y.-K. Baek and P.-W. Shin, *Composites, Part A*, 2017, **98**, 184–191.
33 W. C. Bian, T. Yao, M. Chen, C. Zhang, T. Shao and Y. Yang, *Compos. Sci. Technol.*, 2018, **168**, 420–428.
34 D. X. Zou, X. Y. Huang, Y. K. Zhu, J. Chen and P. K. Jiang, *Compos. Sci. Technol.*, 2019, **177**, 88–95.
35 T. Huang, C. Ma, P. Dai and J. Zhang, *Compos. Sci. Technol.*, 2019, **176**, 46–53.
36 C. Pan, K. Kou, Y. Zhang, Z. Li, T. Ji and G. Wu, *Mater. Sci. Eng., B*, 2018, **238–239**, 61–70.
37 M. C. Vu, T. S. Tran, Y. H. Bae, M. J. Yu, V. C. Doan, J. H. Lee, T. K. An and S.-R. Kim, *Macromol. Res.*, 2018, **26**, 521–528.
38 R. Qian, J. H. Yu, C. Wu, X. Zhai and P. K. Jiang, *RSC Adv.*, 2013, **3**, 17373–17379.
39 Y. Z. Feng, C. G. He, Y. F. Wen, X. P. Zhou, X. L. Xie, Y. S. Ye and Y. W. Mai, *Compos. Sci. Technol.*, 2018, **160**, 42–49.
40 L. Cao, J. J. Wang, J. Dong, X. Zhao, H. B. Li and Q. H. Zhang, *Composites, Part B*, 2020, **188**, 107882–107891.
41 G. Zhang, L. Fan, L. Bai, M. He, L. Zhai and S. Mo, *Chin. J. Polym. Sci.*, 2018, **36**, 1394–1402.
42 D. Ding, H. Wang, Z. Wu, Y. Chen and Q. Zhang, *Macromol. Rapid Commun.*, 2019, **40**, 1800805–1800810.
43 H.-D. Wang, B. Cao and Z. Guo, *Int. J. Heat Mass Transfer*, 2010, **53**, 1796–1800.
44 J. Gu, Z. Lv, Y. Wu, Y. Guo, L. Tian, H. Qiu, W. Li and Q. Zhang, *Composites, Part A*, 2017, **94**, 209–216.
45 W. Yang, R. Luo, Z. Hou and H. Shang, *Vacuum*, 2016, **132**, 95–105.
46 M. Lin, Y. Li, K. Xu, Y. Ou, L. Su, X. Feng, J. Li, H. Qi and D. Liu, *Compos. Sci. Technol.*, 2019, **175**, 85–91.